P3.1 Extending the capabilities of the polarimetric WSR-88D: Observations of cirrus clouds and moist layers

Valery Melnikov[+], Phillip Chilson[~], and David Mechem[*]

[+] Cooperative Institute for Mesoscale Meteorological Studies, University of Oklahoma, Norman, OK.
[~] School of Meteorology, University of Oklahoma, Norman, OK.
[*] Department of Geography, University of Kansas.

1. Introduction

Clouds are one of the main components of the water cycle and radiation balance in the atmosphere. Large amounts of cloud data have been obtained with mm-wavelength cloud radars. X-band weather radars (3-cm wavelength) have been used for cloud studies and precipitation measurements in light and moderate rain. Weather radars with wavelengths longer than 5 cm are successfully used to measure precipitation and monitor severe weather; no such radars are used for cloud sounding.

MM-wavelength cloud radars have detectability of -25-35 dBZ at 10 km to get information on various types of non precipitating clouds (Clothiaux et al. 1995, Stephens et al. 2002). To use weather radar for cloud sounding, such detectability should be achieved for weather radars. In the next section, we describe a technique that brings sensitivity of the networking WSR-88D weather radar to a level of cloud radars. Enhanced sensitivity of the WSR-88D permits detection of many types of non-precipitating clouds (Melnikov et al. 2007) including cirrus clouds (next section herein). This information could be used in parameterization of cloud models and radiation transfer problems in the atmosphere.

Enhanced radar detectability allows also observations of atmospheric layers of increased humidity under "clear are" conditions (section 4), i.e., wherein the layers are not masked by clouds located at same height. We have conducted our experiments on the polarimetric WSR-88D KOUN situated in central Oklahoma (Norman, OK). The main goal of the experiments was to detect moist layers in the atmosphere for its possible use in forecasting of convection.

2. Radar observations of weakly reflecting clouds

WSR-88Ds are operated in two surveillance modes: "clear air" and "precipitation". The "clear air" mode is used in fair weather to monitor possible development of precipitation. In this mode, a microwave 4.5 μs pulse is transmitted (750 m range resolution) to improve the detection of weak echoes. Radar measurements are performed in "precipitation" mode with 1.54 μs radar pulse (250 m range resolution). To enhance quantitative measurements of clouds, the following data collection and signal processing procedures were used:

1) Dwell time of about 120 ms (i.e., 128 samples spaced a bit less than 1 ms apart at the pulse repetition frequency of 1013 Hz) to improve accuracy of measurements and suppress noise,
2) Small elevation increments of 0.25^o to improve accuracy and number of measurements,
3) Twice the range sampling rate, also to suppress noise,
4) A noise speckle remover to reduce the occurrence of false echoes,
5) Correlation estimators for polarimetric variables to mitigate noise effects,
6) Data collection at elevations higher than 20^o to observe clouds at close range, and
7) Ground clutter filters at all elevations to lessen clutter influence.

These procedures allow clear data presentations at SNR as low as -7 dB. For the KOUN, Z_{10}, presented in the non-polarimetric mode and short radar pulse, is -21.5 dBZ (Table 1). The enhanced signal processing permits measurements of -28.5 dBZ. The long radar pulse adds more 4.8 dB to sensitivity bringing it to level of -33 dBZ@10 km. This sensitivity is on par with one of the cloud radars. Radar parameters of the operational MMCR cloud radar operated by the Atmospheric Radiation Measurements program and WSR-88D are compared in Table 1. It is seen from the table that Z_{10} of KOUN is close to the one of MMCR, but KOUN has a larger radar volume. So KOUN with enhanced signal processing is capable of observing light non precipitating clouds.

Valery.Melnikov@noaa.gov

Table 1. Radar parameters

	MMCR	WSR-88D
Wavelength (mm)	8.7	109
Antenna beamwidth, (deg.)	0.2	0.96
Radial resolution (m)	45 / 90	250 (short pulse)
Two-way transversal resolution (m)	17@10 km	82@10 km;
Z_{10} (dBZ)	-30 (general and stratus modes)	-25.5 (enhanced processing in dual-pol, short pulse), -28.5 (enhanced processing, single pol., short pulse), -33.3 (enhanced processing in single-pol, long pulse)
Scanning capability	No	Yes
Dual Polarization	Yes for the SGP site	Yes for KOUN. Yes for upgraded WSR-88Ds.

Fig.1 demonstrates the capability of the KOUN to detect optically thin clouds.

A sky picture towards the East-North-East from KOUN is presented in Fig. 1(a). At the same time, KOUN reflectivity from vertical cross-sections at azimuth 180^o is shown in the right panel. Cloud radar echo is circled with red in Fig. 1(b). Examples of observations of cirrus clouds are presented in Figs. 2 and 3. WSR-88D KTLX located 11 km North-East of KOUN was not capable to detect the clouds. In visible satellite images (not shown), the clouds are barely seen in central Oklahoma. KOUN detects the clouds to 50 km; the heights and thickness of the clouds can be measured. Ground clutter filter residuals contaminate the data to 5-7 km, beyond that they are sporadic and do not impose significant problems to cloud mapping. Boundary layer reflectivity is clearly observed at all distances. An example of cirrus clouds above precipitation is shown in Fig. 4.

It should be noted that the short radar pulse is used to produce radar images in Figs. 1-3. To detect low altitude and weakly reflecting clouds, the long-pulse mode can be utilized; this adds about 4.5 dB to sensitivity. Then Z_{10} reaches -30 dBZ in the dual-polarization mode. The polarimetric WSR-88D will be capable of injecting its total transmitted power into a single polarization; this will decrease Z_{10} to a level of -33 dBZ. Thus the WSR-88D has a detection capability that exceeds some mm-wavelength cloud radars. Radar observations of clouds can significantly compliment satellite data by supplying a more complete description of cloud structures, altitudes of the tops and bottoms, and wind velocities in clouds.

To obtain the optical thickness of clouds in Figs. 2 and 3, we have compared measured solar radiation on the ground with model results. To estimate solar flux on the ground, we have used the Bird model (Bird and Hustorm, 1981). The Oklahoma mesonet measures solar radiation every 5 minutes. We obtained data from a mesonet site located in Norman, OK. For the time represented in Fig.2, the measured and modeled solar radiation were 751 and 797 W/m^2. That is, the clouds absorbed less than 6% of the solar radiation and thus they were optically thin. For the time represented in Fig. 3, the measured solar radiation was 427 W/m^2 and the model value is 395 W/m^2, i.e., less that measured. Such an excess is observed on partially cloudy days. We conclude that the WSR-88Ds can observe radiative significant clouds.

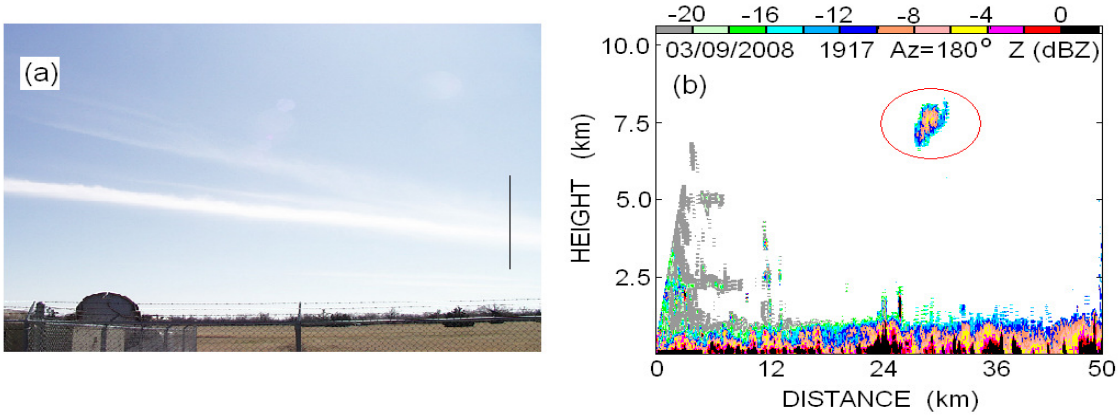

Fig. 1. 9 March 2008. (a): Sky picture from KOUN at 1918 UT. The vertical black line is the direction of the radar reflectivity cross section shown in panel (b). Radar echo from the cloud is circled.

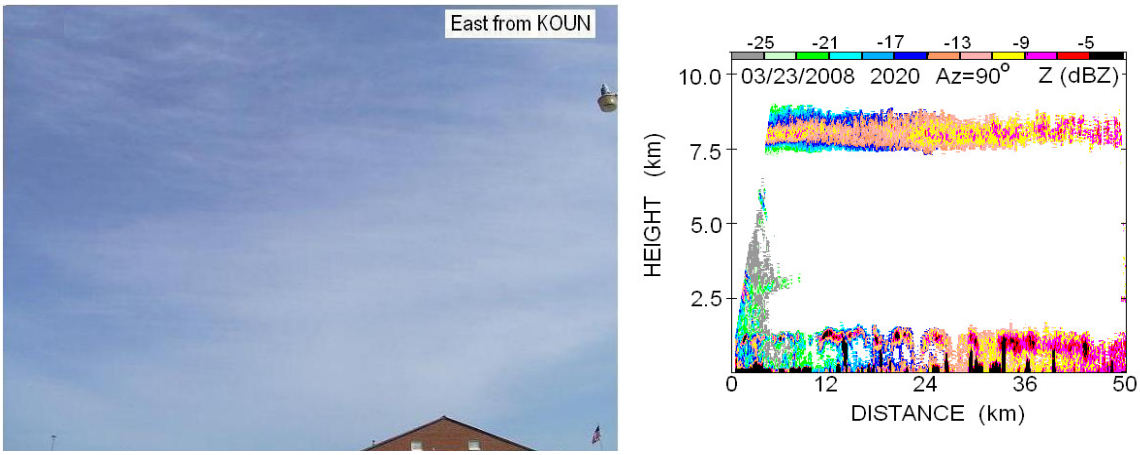

Fig. 2. 23 March 2008. (Left): Sky picture from KOUN at 2021 UT looking toward the East. (Right): Vertical cross section of reflectivity factors observed with KOUN.

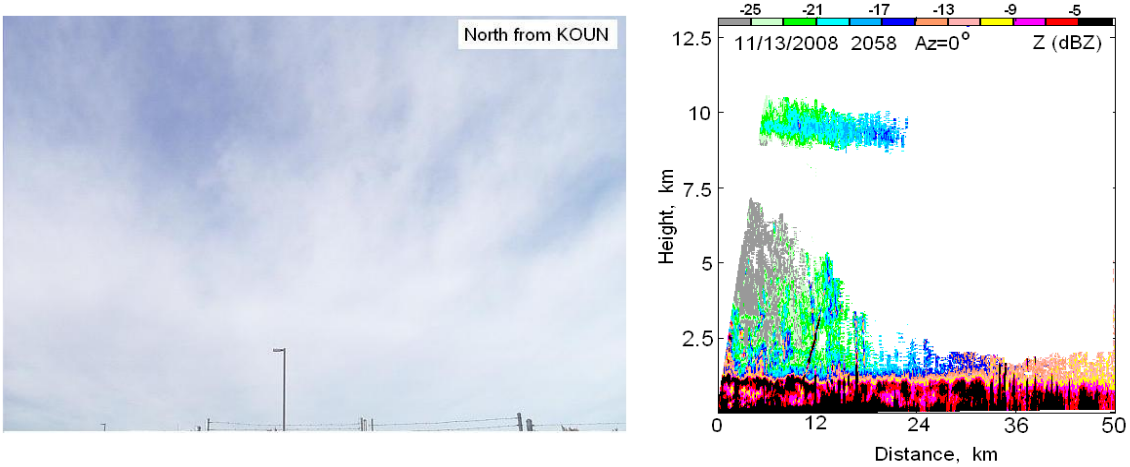

Fig. 3. 13 November 2008. (Left): Sky picture from KOUN at 2100 UT looking toward the North and (right) the vertical cross section of reflectivity factors observed with KOUN at azimuth 0°.

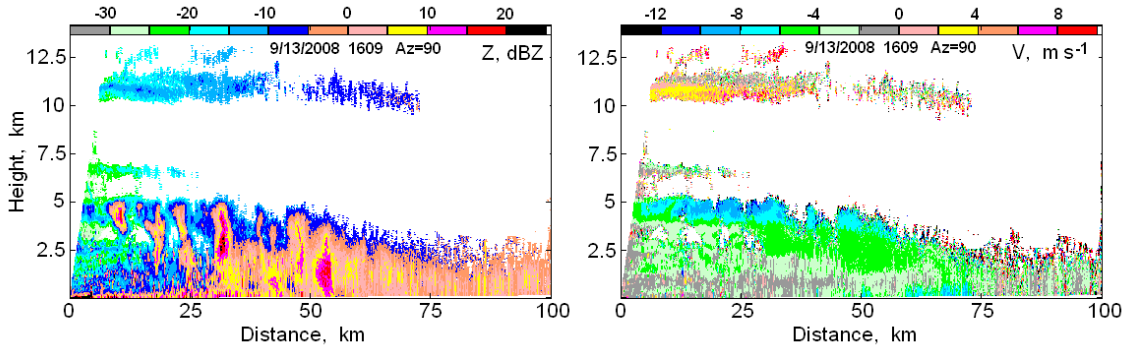

Fig. 4. Cirrus clouds above precipitation: (left) reflectivity and (right) the Doppler velocity fields.

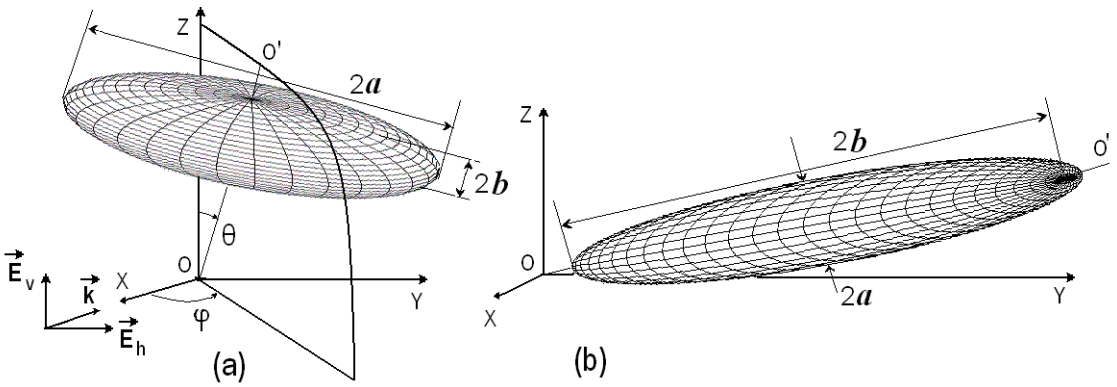

Fig. 5. Oblate (a) and prolate (b) spheroidal scatterers and the incident waves.

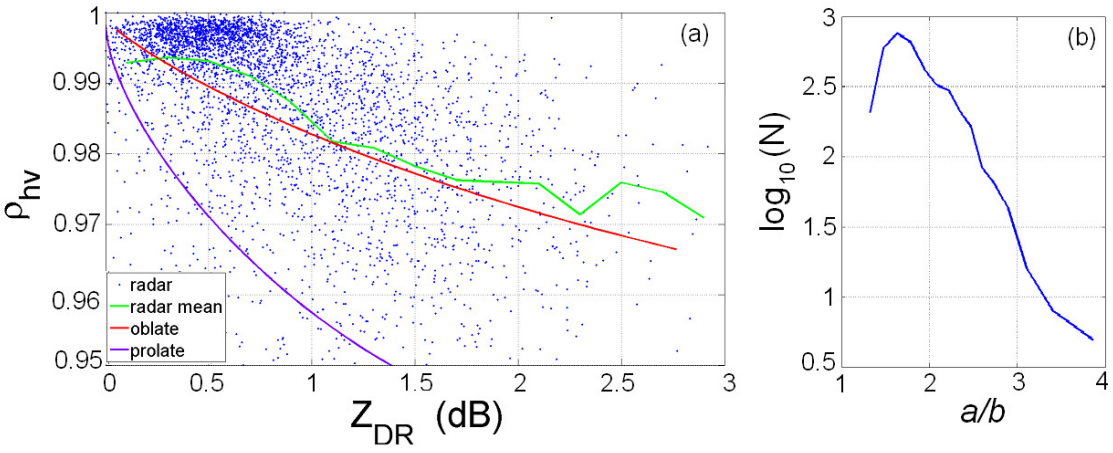

Fig.6. (a): Relations between Z_{DR} and ρ_{hv} in clouds at height of 5 km. The dots are radar data, the green line is the mean of the radar data, the red and blue lines are the mean dependencies for oblate and prolate particles correspondingly obtained via (6). (b): The relative number concentration of particles as a function of the aspect ratio *a/b*.

3. Z_{DR} – ρ_{hv} relation and particles' shapes in clouds

Radar polarimetric observations can be used to estimate the shape of cloud particles. Fields of polarimetric variables in nonprecipitating clouds are complicated due to variety of ice crystal habits. Matrosov et al. 1996, 2001 and Reinking et al. 2002 utilized depolarization measurements at X band (radar wavelength is 3.2 cm) to obtain types and shapes of ice hydrometeors. Signal in the orthogonal radar channel is 10-20 dB weaker than the signal in the copolar channel. Thus such measurements can be carried out in thick clouds wherein depolarized signal is strong. In this paper, we consider weakly reflecting clouds in which depolarization cannot be measured with KOUN (S frequency band, wavelength is 11 cm). Consider utilization of differential reflectivity, Z_{DR}, and the copolar correlation coefficient, ρ_{hv}, that are measured with KOUN, to estimate shapes of ice crystals. Parameters of backscattered radar radiation depend on the sizes and shapes of cloud particles, their orientation relative to incident waves, and the particles' dielectric permittivity.

Sizes and shapes. Cloud particles are much smaller than the radar wavelength, i.e., 11 cm, so that the Raleigh approximation for backscattering cross-sections is applicable. Cloud particles can be of different shapes which are close to columns, plates, rosettes, dendrites, or aggregates. In high altitude clouds such as cirrus, the main process of particles growth is vapor deposition (Pruppacher and Klett, 1978) thus aggregates can be excluded. The rest shapes can be approximated by two major shape types: oblate and prolate spheroids. Columnar crystals are close to prolate spheroids. Plates and dendrites can be considered as oblate spheroids. We consider herein spheroids, i.e., scatterers with rotational symmetry. Such particles are characterized with two semi-axes a and b as it is shown in Fig. 5.

Dielectric properties of cloud particles at centimeter wavelengths is taken as for solid ice, i.e., $\varepsilon = 3.15$, because the main growth process of particles is deposition of water vapor.

Orientation of cloud particles is preferably horizontal as it is concluded from positive differential reflectivities. Nonuniformities of the wind destroy horizontal orientation of the particles so that they can be characterized by an angle distribution relative to the horizontal plane. Orientation of a particle can be characterized with two Euler angles θ and φ which are shown in Fig. 5. We use herein a completely random distribution in φ, i.e., the uniform distribution. To perform averaging in θ for oblate particles, we consider the uniform distribution in θ from 0 to some θ_o, which is a model parameter. We will refer θ_o to as the maximal "flutter" angle. The completely random distribution in θ corresponds to $\theta_o = 90^o$.

Formulation of the model. Geometry of the particles and incident waves are sketched in Fig. 5. The propagation direction of the radio waves is determined by vector $\vec{k}$ that lies along the x-axis. OO' is the axis of rotation of the spheroids. For oblate plate-like scatterers, $b< a$ and for prolate needle-like particles, $b> a$. We consider horizontal sounding which is a good approximation for elevation angles lower than 20^o. Transmittion of polarized radio-waves, their scattering by particles, and reception of the scattered waves can be described by the following matrix equation (e.g., Doviak and Zrnic, 2006, 8.5.2.1):

$$\begin{pmatrix} E_{hr} \\ E_{vr} \end{pmatrix} = \begin{pmatrix} S_{hh} & S_{hv} \\ S_{hv} & S_{vv} \end{pmatrix} \begin{pmatrix} E_h \\ E_v \end{pmatrix}, \qquad (1)$$

where S_{ij} are the scattering coefficients of the medium. In (1) range dependence and radar constants are omitted without loss of generality because we are interested in polarimetric parameters that do not depend on those. Powers P_h and P_v in the receive channels and the correlation function R_{hv} between received waves are:

$$P_h = <|E_{hr}|^2>, \qquad P_v = <|E_{vr}|^2>,$$
$$R_{hv} = <E_{hr}^* E_{vr}>, \qquad (2)$$

where the brackets stand for ensemble averaging and the asterisk denotes the complex conjugate. From (2), the differential reflectivity Z_{DR}, the differential phase shift φ_{dp} and the copolar correlation coefficient ρ_{hv} are obtained

$$Z_{DR} = 10\log Z_{dr}, \qquad Z_{dr} = \frac{P_h}{P_v}, \qquad (3a)$$

$$\rho_{hv} = \frac{|R_{hv}|}{(P_h P_v)^{1/2}}, \qquad \varphi_{dp} = \arg(R_{hv}) \qquad (3b)$$

The matrix coefficients for n-th scatterer in (1) are

$$S_{hh}^{(n)} = \alpha_a + \Delta\alpha \sin^2\theta \ \sin^2\varphi,$$
$$S_{hv}^{(n)} = \Delta\alpha \ \sin\theta \ \cos\theta \ \sin\varphi, \qquad (4a)$$

$$S_{vv}^{(n)} = \alpha_a + \Delta\alpha \ \cos^2\theta \ ,$$
$$\Delta\alpha = \alpha_b - \alpha_a \ , \qquad (4b)$$

where α_a and α_b are the polarizabilities along a and b (e.g., Bringi and Chandrasekar, 2001, Eq. (2.53)). To get S_{ij} in (1), we have to sum up (4) for all scatterers in the radar volume

The calibration procedure takes care of difference in transmitted amplitudes E_h and E_v in (1) so we can assume that they are equal and omit them. Using (1), the received voltage from n-th scatterer in the radar volume can be represented as

$$E_{hr}^{(n)} = \alpha_a + \Delta\alpha \sin^2\theta \ \sin^2\varphi + \Delta\alpha \sin\theta \ \cos\theta \ \sin\varphi \ , \qquad (5a)$$

$$E_{vr}^{(n)} = \Delta\alpha \sin\theta \ \cos\theta \ \sin\varphi + (\alpha_a + \Delta\alpha \cos^2\theta) \ . \qquad (5b)$$

The distribution in φ can be considered uniform with high confidence. Assuming independence of the φ- and θ-distributions, we obtain $<\sin^2\varphi>=1/2$; then substitution of (5) into (1) yields

$$P_h = <|\alpha_a|^2> + \mathrm{Re}(<\alpha_a \Delta\alpha^*>) J_1 + \frac{1}{8} <|\Delta\alpha|^2> (4J_1 - J_2) \ , \qquad (6a)$$

$$P_v = <|\alpha_a|^2> + \mathrm{Re}(<\alpha_a \Delta\alpha^*>)(1 - J_1) + \frac{1}{2} <|\Delta\alpha|^2> (2 - 3J_1 + J_2) \qquad (6b)$$

$$R_{hv} = e^{i\psi_r} \{ [<|\alpha_a|^2> + <\alpha_a^* \Delta\alpha>)(1 - J_1) + \frac{1}{2} <\alpha_a \Delta\alpha^*> J_1] e^{i\psi_t} + |\Delta\alpha|^2 (J_1 - J_2) \cos\psi_t \}, \qquad (6c)$$

$$J_1 = <\sin^2\theta>, \qquad J_2 = <\sin^4\theta> , \qquad (6d)$$

where $\mathrm{Re}(x)$ stands for the real part of x, ψ_t is the system differential phase on transmit, and the brackets around the polarizabilities denote size averaging. At S-band, cloud particles can be considered as Rayleigh scatterers and the polarizabilities for oblate scatterers ($a \geq b$) are (e.g., Bohren and Huffman 1983, section 5.3):

$$\alpha_a = \frac{4}{3}\pi \ a^2 b \frac{\varepsilon - 1}{1 + L_a(\varepsilon - 1)} \ ,$$
$$\alpha_b = \frac{4}{3}\pi \ a^2 b \frac{\varepsilon - 1}{1 + L_b(\varepsilon - 1)} \ , \qquad (7)$$
$$L_a = \frac{g}{2e^2}\left(\frac{\pi}{2} - \tan^{-1} g\right),$$
$$L_b = 1 - 2L_a, \ \ g = \left(\frac{1 - e^2}{e^2}\right)^{1/2} \ , \ .$$
$$e^2 = 1 - (b/a)^2$$

For prolate scatterers, (7) holds as well with $b \geq a$ and

$$L_b = \frac{1 - e^2}{e^2}\left(\frac{1}{2e} \ln\frac{1 + e}{1 - e} - 1\right), \qquad L_a = 0.5(1 - L_b), \qquad e^2 = 1 - (a/b)^2 \ .$$

Radar quantities in (6) are the means so we use (7) for the "mean" particle.

To perform averaging in θ for oblate particles, we consider the uniform distribution in θ from 0 to some θ_o, which is a model parameter. To get a relation between Z_{DR} and ρ_{hv} for oblate particles, we assume that the flatter angle increases with decreasing oblateness, so that spherical particles rotate arbitrary in φ and θ but oblate particles are more stable at wobbling and have their own flatter angle θ_o that linearly depends on oblateness parameter b/a, i.e.,

$$\theta_o, = 70 \ b/a + 20 \ (\mathrm{deg}). \qquad (8)$$

For very oblate particles, i.e., $b/a \ll 1$, the particles wobble with the flatter angle of 20° so that the mean angle is 10° which is close to the flatter angle for raindrops.

Radar data. In Fig. 6(a), a Z_{DR} - ρ_{hv} scattergram of radar data are presented for heights 5 km (the dots) with temperatures about -17°C. The data have been collected from nonprecipitating clouds from radar volumes with SNR >= 10dB. The mean dependency for data is shown with the green line. The mean Z_{DR} - ρ_{hv} relations calculated via (6) are shown with the red (oblate particles) and blue (prolate particles) lines. It is seen that the calculated curve for oblate particles is close to the mean radar data so we can conclude that the cloud particles at this height have oblate shapes. The

latter is in accord with cloud data for temperature interval -15..-20 ^{o}C (Pruppacher and Klett, 1978, 2.2).

Radar data in Fig. 6(a) can be used also to estimate relative number concentration for particles having a given aspect ratio, i.e., a/b. Neither Z_{DR} nor ρ_{hv} depend on the absolute number concentration but Fig. 6(a) demonstrates a dependency of the number of particles having given differential reflectivity. It is seen that vast majority of the measurements has Z_{DR} near 0.5 dB. According to (6a,b), each point on the red line in Fig. 6 corresponds to a certain aspect ratio. Using this correspondence, the relative number concentration can be obtained. The result is shown in Fig. 6(b). One can see that vast majority of particles has the aspect ratio near 1.6. It seen also that particles with $a/b > 3.5$ are present in the radar volume with the relative number concentration 3 order of magnitude less than those with $a/b \approx 1.6$.

4. **Polarimetric radar observations of moist layers**

Enhanced sensitivity of KOUN radar allows detecting echoes from "clear" air, i.e., in the absence of precipitation and clouds. Observations show that such echoes are located in the boundary layer and have shapes of layers. Radar panels in Figs. 1-3 clearly demonstrate that KOUN detects reflections from the boundary layer. Such echoes are areas of enhanced refractivity related to increased humidity and they are usually detected with vertically pointed wind profilers (e.g., Doviak and Zrnic 2006). On scanning WSR-88Ds with enhanced signal processing, temporal-spatial observations of moist layers are possible. Often, clear air echoes exhibit bubble structures as in Figs. 2 (right) and 7 (right). Examples of elevated layers are shown in Figs.7, 8, and 10.

Rawindsonde profiles taken from KOUN corresponding to the nearest sounding time (or times) show that cloud and moist layers detected by radar are accompanied by increased humidity, relative to layers above and below (Figs. 7, 8, and 10). We note that Figs. 8 and 10 particularly illustrate the drawbacks of launching only two soundings per day in meteorological situations that are rapidly evolving.

In the cold season in Oklahoma, insects do not contaminate clear air radar returns so polarimetric measurements of moist layers are possible. An Example of observations with KOUN is shown in Fig. 8. Distributions of measured polarimetric variables are presented in Fig. 9. Radar returns from moist layers are weak so significant fluctuations of measured parameters should be expected. This is seen from Fig. 9: instantaneous values of Z_{DR} lays in interval – 1 to 1 dB and values of ρ_{hv} are in interval 0.95 to 1.05. Estimates of ρ_{hv} exceeding unity are possible for weak signals. Symmetry of the distributions signify their statistical nature thus their mean values can be attributed to polarimetric properties of scattering media. So we conclude from Fig. 9 that differential reflectivity from moist layer is close to 0 dB and the copolar correlation coefficient is unity. This conclusion is in accord with intuitive expectations on reflection of radio waves from turbulent moist air.

Zero Z_{DR} in moist layers can be used to check calibration of a polarimetric radar. Polarimetric schemes with simultaneous transmission and reception of electromagnetic waves at orthogonal polarization planes require measurements of the system differential reflectivity. The latter is a result that a dual-polarization radar has two physically different channels with different gains (Zrnic et al. 2006). So this difference must be accounted for with the system differential reflectivity. Measurements of differential reflectivities from boundary layer, i.e., $Z_{DR} = 0$ dB, can be utilized to check the system differential reflectivity. This can be done in cold season wherein no insects are present in the atmosphere.

In the presence of insects, moist layers are observed as areas of decreased Z_{DR} and increased ρ_{hv} as in Fig.10. It is seen that in the reflectivity field, it's hard to recognize a moist layer. Insects exhibit strong positive Z_{DR}. A layer of decreased ZDR in Fig. 10 manifests the presence of a moist layer which shifts Z_{DR} values from high "insect" Z_{DR} down to zero Z_{DR} pertinent to clear air. This is supported by shifting of ρ_{hv} up in the layer of decreased Z_{DR}. Shifting of ρ_{hv} up is caused by reflection from moist air that has correlation coefficients close to unity. Rawindsonde profiles taken from KOUN corresponding to the nearest sounding time (or times) show that cloud and moist layers detected by radar are accompanied by increased humidity, relative to layers above and below (Figs. 7, 8, and 10). Although we have not formally calculated refractivity, we suspect that some of these "moist" radar echoes are associated with refractivity gradients captured in the soundings, in addition simply to layers of anomalously high humidity. We note that Figs. 8 and 10 particularly illustrate the drawbacks of launching only two soundings per day in meteorological situations that are rapidly evolving.

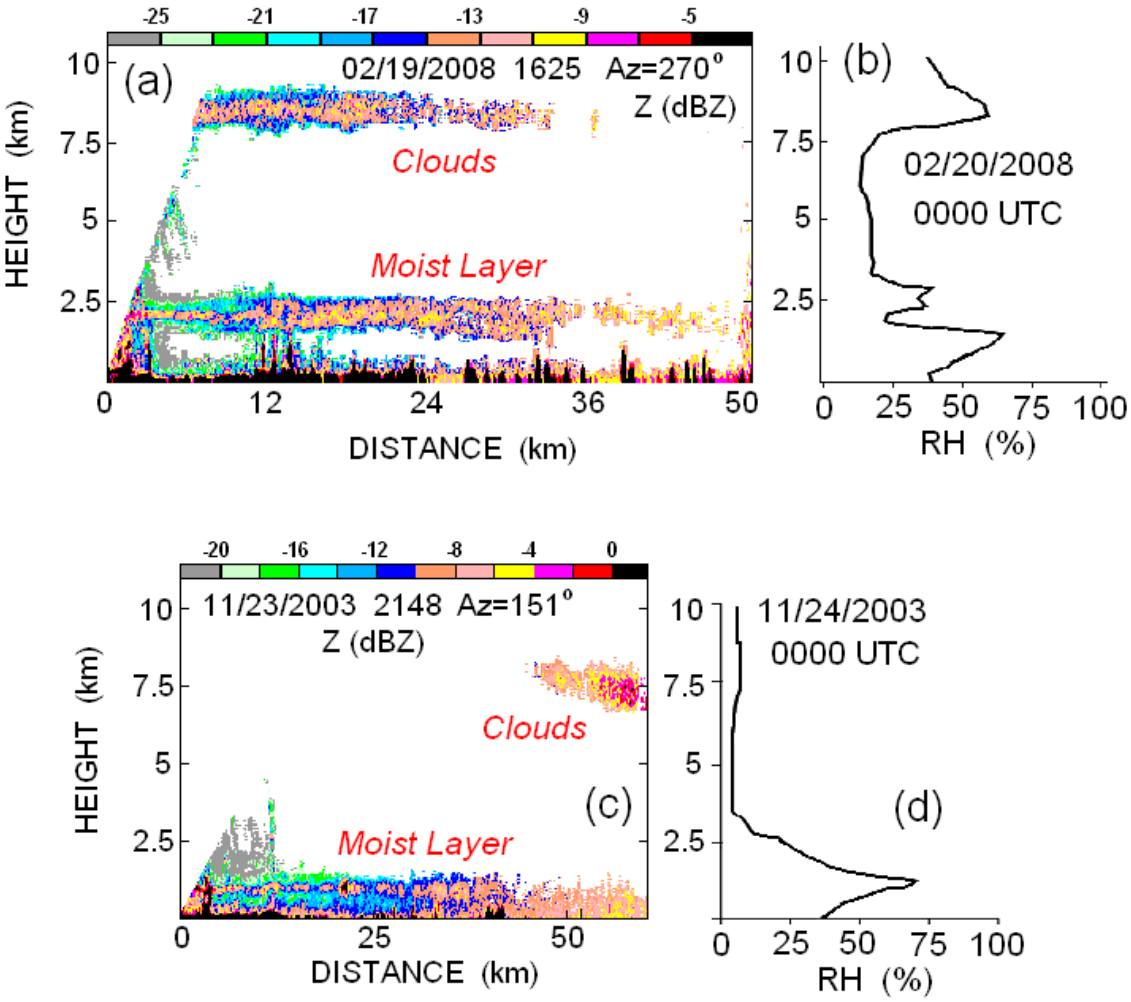

Fig. 7. (a,c): Reflectivities of clouds and moist layers observed with KOUN.
(b,d): Profiles of relative humidity, RH, obtained from nearest soundings in time.

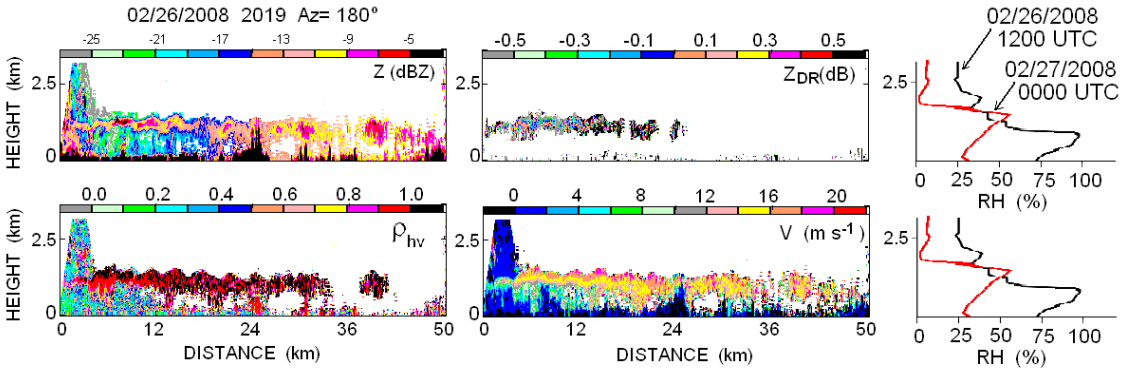

Fig. 8. Wave-like elevated moist layer with maximal reflectivities about -3 dBZ. Profiles of relative humidity are depicted in the right panels.

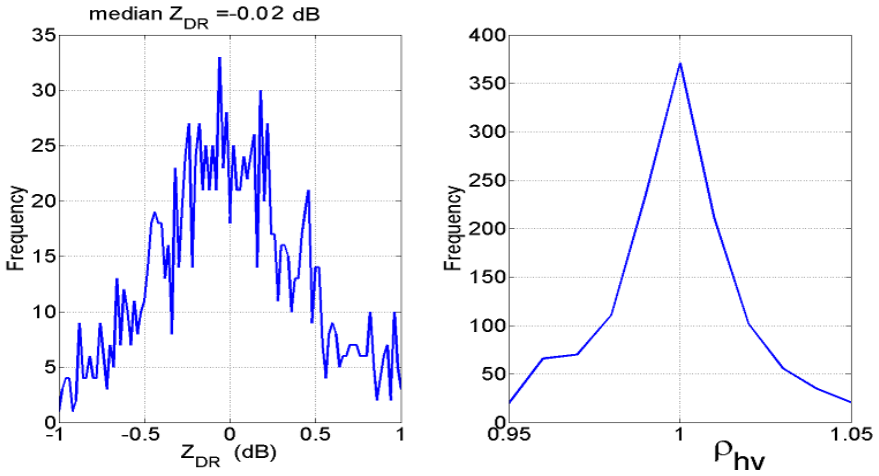

Fig. 9. Distributions of Z_{DR} and ρ_{hv} in the moist layer shown in Fig. 8.

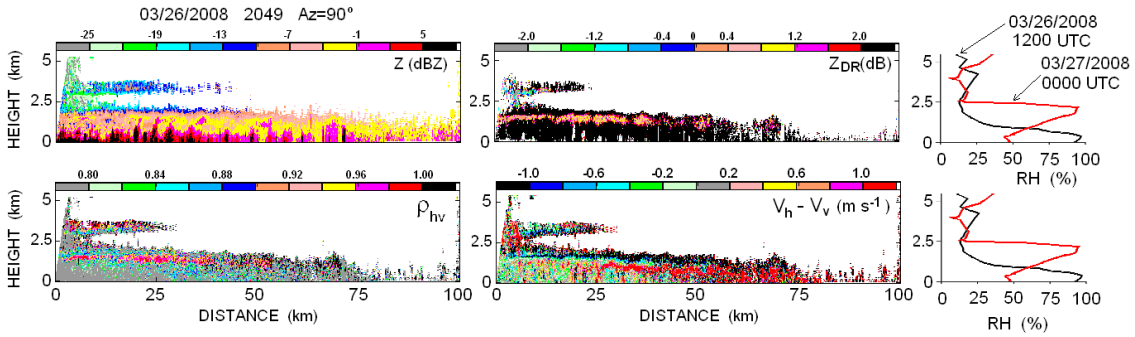

Fig. 10. Moist layer at the height of 1.8 km imbedded into echo from insects. The V_h - V_v panel is the difference of radar Doppler velocities measured at horizontal and vertical polarizations. Profiles of relative humidity are depicted in the right panels.

Conclusions

- The enhancements to signal processing allows observing of nonprecipitating clouds with reflectivities of -25.5 dB that permits radar observations of some types of cirrus. This sensitivity is for dual polarization measurements with the short radar pulse. Radar observations of weakly reflecting clouds can be used for climatological studies, cloud models, and problems of radiation in the cloudy atmosphere. We demonstrated the optically significant clouds can be observed with the WSR-88D (Figs. 2,3).

- $Z_{DR} - \rho_{hv}$ relations in clouds can be used for estimation of the mean shape of cloud scatterers. This shape is for largest particles that make strongest contribution to the backscattered radar signal. Presented radar data is in an agreement with plate-like shapes of cloud particles at heights of 5 km. $Z_{DR} - \rho_{hv}$ relation in clouds allow obtaining a distribution of particles in the aspect ratio, i.e., the ratio of major and minor axis.

- Increased radar detectability allows observations of moist layers in the atmosphere. With KOUN, moist layers with maximum equivalent reflectivities about – 3 dBZ have been observed. Observations of moist layers with scanning radars permit spatial-temporal monitoring of the layers. Waviness and "bubbleness" of the layer indicate that convection has a strong impact on the layers.

- Differential reflectivity and the copolar correlation coefficients in moist layers in cold seasons (free from insects) are close to zero and one correspondingly. Closeness of Z_{DR} to zero in moist layers can be used to check radar calibration of differential reflectivity. In moist layers imbedded in insect echoes, we observe slightly positive differential reflectivities which could be due to contamination of clear air signal with echoes from insects.

References

Bird, R. E., and R.L. Hulstrom, 1981: A simplified clear sky model for direct and diffuse insolation on horizontal surfaces. SERI reports, SERI/TR-642-761, 39 pp.

Bohren, C.F., and D.R. Huffman, 1983: *Absorption and Scattering of Light by Small Particles* , John Whilley and Son, San Diago, CA, 457 pp.

Clothiaux, E.E., M.A. Miller, B.A. Albrecht, T.P. Ackerman, J. Verlinde, D.M. Babb, R.M. Peters, and W.J. Syrett, 1995: An evaluation of a 94-GHz radar for remote sensing of cloud properties. *J. Atmos. Oceanic Technol.*, 12, 201-229.

Doviak, R. J. and D. S. Zrnic, 2006: *Doppler radar and weather observations*, 2nd ed., Academic Press, 562 pp.

Matrosov, S. Y., R.F. Reinking, R.A. Kropfli, and B. W. Bartram, 1996: Estimation of ice hydrometeor types and shapes from radar polarization measurements. *J. Atmos. Oceanic Technol.*, 13, 85-96.

Matrosov, S. Y., R.F. Reinking, R.A. Kropfli, B. E. Martner, and B.W. Bartram, 2001: On the use of radar depolarization ratios for estimating shapes of ice hydrometeors in winter clouds. *J. Applied Meteorol.,* 40, 479-490.

Melnikov, V.M., D.S. Zrnic, R.J. Doviak, Y.L. Kogan, P. B. Chilson, and D.B. Mechem, 2007: The WSR-88D observes nonprecipitating clouds. 33rd Weather Radar Conf., Cairns, Australia, P6A.3.

Pruppacher, H.R., and J.D. Klett, 1978: *Microphysics of clouds and precipitation.* D.Reidel Publ. Co., Boston, 714 pp.

Reinking, R.F., S.Y. Matrosov, R.A. Kropfli, and B. W. Bartram, 2002: Evaluation of a 45° slant quasi-Linear radar polarization state for distinguishing drizzle droplets, pristine ice crystals, and less regular ice particles. *J. Atmos. Oceanic Technol.*, 19, 296-321.

Stephens G. L, D.G. Vane, R.J. Boain, G.G. Mace, K. Sassen, Z. Wang, A. J. Illingworth, J. O'Connor, W. B. Rossow, S.L. Durden, S.D. Miller, R.T. Austin, A. Benedetti, C. Mitrescu, 2002: The CLOUDSAT mission and the A-train. *Bull. Amer.Meteor. Soc.,* Dec, 1771-1790.

Zrnic, D.S., V.M. Melnikov, and J.K.Carter, 2006: Calibrating differential reflectivity on the WSR 88D. *J. Atmos. Oceanic Technol.,* 23, 944-951